Area determination with pile-up and sink-in in nanoindentation of oxygen containing titanium

Kværndrup, Frederik B.; Engelbrekt, Christian; Kücükyildiz, Ömer C.; Somers, Marcel A.J.; Christiansen, Thomas L.; Winther, Grethe

Published in:
Materials Today Communications

Link to article, DOI:
10.1016/j.mtcomm.2022.103218

Publication date:
2022

Document Version
Publisher's PDF, also known as Version of record

Materials Today Communications 30 (2022) 103218

Contents lists available at ScienceDirect

Materials Today Communications

journal homepage: www.elsevier.com/locate/mtcomm

Area determination with pile-up and sink-in in nanoindentation of oxygen containing titanium

Frederik B. Kværndrup [a,b,*], Christian Engelbrekt [a,c], Ömer C. Kücükyildiz [a,b], Marcel A. J. Somers [a,b], Thomas L. Christiansen [a,b], Grethe Winther [a,b]

[a] Technical University of Denmark, DK 2800 Kgs. Lyngby, Denmark
[b] Department of Mechanical Engineering, Denmark
[c] Department of Chemistry, Denmark

ARTICLE INFO

Keywords:
Interstitial alloys
Mechanical properties
Atomic force microscopy
Elasticity
Anisotropy

ABSTRACT

Homogenous thin foils of titanium with oxygen in interstitial solid solution covering the broad solubility range of O in h.c.p. Ti, were used to investigate the sink-in and pile-up occurring during nanoindentation. The anisotropic response and indent areas were accurately analyzed with atomic force microscopy. The mechanical properties and the indent areas were assessed using both the Oliver&Pharr method and a newer method incorporating corrections for indenter geometry and an improved parameter extraction. The newer method accurately accounts for pile-up.

1. Introduction

The probing of the mechanical properties of a wide variety of materials has been performed using instrumented nanoindentation since the 1990′s, with the method developed by Oliver&Pharr (OP) being the most widely used [1]. Nanoindentation allows for the detection of plastic and elastic properties based on an experimental setup, which is described in more detail in [2,3]. The method involves the pressing of a 3-sided pyramidal Berkovich indenter into a plane surface, and recording the resultant applied force versus penetration depth curve. The validity of the obtained results depends strongly on the accuracy with which the projection of the contact area on the sample surface is determined [4]. The area dependence for the hardness, reduced indentation modulus and indentation modulus is given in equations 1.1, 1.2 and 1.3, respectively [1].

$$H = \frac{P_{max}}{A} \tag{1}$$

$$E_r = \frac{\sqrt{\pi} \bullet S}{2 \bullet \sqrt{A}} \tag{2}$$

$$\frac{1}{E_r} = \frac{(1-\nu^2)}{E} + \frac{(1-\nu_i^2)}{E_i} \tag{3}$$

where P_{max}, H, A, E_r, S, E and ν are the max force, hardness, projected contact area, reduced indentation modulus, slope of the unloading curve, Young's modulus and Poisson's ratio, respectively. The E_i and ν_i are the parameters for the indenter. For an ideal Berkovich tip the projected contact area is a function of the contact depth (h_c) described by the polynomial $A = 24.5 \bullet h_c^2$. Due to the manufacturing or wear of indenter tips the shape may deviate from the ideal one. For this reason, a polynomial of higher order is employed where the coefficients are obtained by fitting to a series of indentation data on fused silica with a known elastic modulus [1]. For example (1−4):

$$A_{Calibration} \quad [nm^2] = 21.21 \bullet h_c^2 + 3549 \bullet h_c - 50309 \tag{4}$$

where the constants are determined for the indenter used in the present experiments. The behavior of the material investigated also affects the contact area. Some materials exhibit pile-up, leaving material on the side of the indent and an increase in indentation area. Others are prone to sink in, resulting in a reduction of the indentation area. The pile-up and sink-in is schematically illustrated in Fig. 1, adapted from [3]. These effects can lead to an error in indentation area of up to 60%, which also adversely affects the hardness and indentation modulus results [5]. Factors affecting the pile-up and sink-in behavior are the ratio between Young's modulus and the yield strength [E/Y], and the material's tendency to work-harden [3]. High E/Y ratios promote pile-up and low

* Corresponding author at: Technical University of Denmark, DK 2800 Kgs. Lyngby, Denmark.
E-mail address: frederikbojsen@gmail.com (F.B. Kværndrup).

https://doi.org/10.1016/j.mtcomm.2022.103218
Received 1 July 2021; Received in revised form 6 January 2022; Accepted 28 January 2022
Available online 2 February 2022

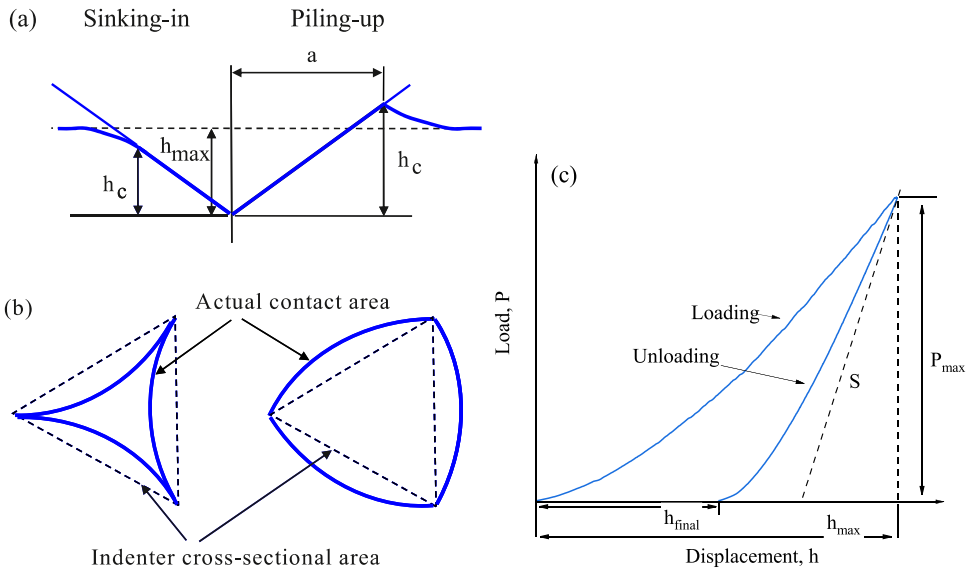

Fig. 1. Schematic overview of sink-in and pile-up from a cross-sectional view (a) and plan view (b). In (a) the indent is under load, whereas (b) shows the indent after unloading. With sink-in and pile-up leading to a reduction or increase in indentation area, respectively. (c) illustrates how Pmax, hmax, hfinal and S are determined from the force-depth curve.
(a) Adapted from [3]. (b) Adapted from [1].

ratios sink-in, in particular in materials with high work-hardening. A useful parameter for predicting pile-up or sink-in is the ratio of the final depth (h_f) to the total depth (h_m), with a ratio above 0.7 indicating pile-up and a ratio below 0.7 suggesting sink-in [5].

The correction of the indentation area for pile-up can either be performed by direct area determination of the final indent using microscopy such as atomic force microscopy (AFM) [6–11] or by analyzing the indentation curve using analytical elastic contact mechanics [2, 12–15]. This analysis accounts for sink-in but does not address pile-up [16]. Improvements have been made by estimating the contact depth from extrapolation of the slope of the initial part of the unloading curve combined with constants describing the indenter geometry [17]. Corrections for pile-up are typically based on finite element modeling (FEM). The latter was demonstrated first by [5] and improved upon by other groups such as Dao et al. (Dao method) [18]. The Dao method is based on a large set of FEM simulations of indentations of materials with E/Y ratios in the range 30–700. Based on these simulations, several dimensionless functions have been determined, which give relations between parameters characterizing the indentation curve (h_f, h_m, the curvature of the loading curve and the slope of the unloading curve) and the material's mechanical properties. The method allows determination of hardness, indentation modulus, yield strength and strain hardening exponent. The focus of the present paper is to investigate sink-in and pile-up and its effect on the indent area and the extracted mechanical properties using three different methods, namely the OP analysis as implemented in the analysis software for the NHT^2 nano-indenter from CSM Instruments,[1] the Dao method extended to employ Eqs. 1–4 in the area determination,[2] and direct measurement of the projected indentation area using AFM. The OP and Dao methods both assume isotropic material behavior while real metals are highly anisotropic and heterogeneous due to the polycrystalline nature. This aspect is, however, beyond the scope of the present study.

As a convenient material for this study, h.c.p titanium with different deliberately dissolved oxygen contents has been selected. The presence of interstitially dissolved oxygen leads to a dramatic increase in the hardness and elastic modulus [22] and is associated with an increase in the c/a ratio of the hcp unit cell. The plastic-elastic behavior changes systematically with the concentration, enabling the measurements of materials with different E/Y and h_f/h_m ratios [19]. H.c.p Ti is also well known to exhibit anisotropic pile-up during nanoindentation [20]. Because oxygen resides interstitially in the octahedrally coordinated interstices, it is most accurate to describe the content in octahedral occupancy, defined as $y_O = \frac{at.\%O}{(100-at.\%O)}$. Hence, the present study investigates oxygen contents covering a broad part of the homogeneity range of Ti-O solid solutions in h.c.p. Ti, i.e. from $y_O = 0.006$ to $y_O = 0.397$(the maximum solubility is $y_O = 0.5$ [21]). It is an extension of a previous study of the effect of interstitially dissolved nitrogen and oxygen in unalloyed titanium [22].

2. Materials and methods

2.1. Synthesis of h.c.p. Ti-O by gaseous thermochemical treatment and vacuum homogenization

The synthesis of the h.c.p Ti-O specimens is described in detail in the preceding study [22], with the 25 μm thick Ti foils selected for this study containing: $y_O = 0.006$, $y_O = 0.021$, $y_O = 0.198$ and $y_O = 0.397$. The Ti foils were oxidized in O_2 (99.99% purity) at 525–725 °C for 1–30 hrs. in a Netzsch STA 449 F3 Jupiter thermal analyzer (TGA). The foils were then homogenized in a custom built Kanthal tube furnace at a vacuum better than $1{\cdot}10^{-6}$ mbar for 50–100 hrs. at 730 °C, realized with an Edwards T-Station 85 pumping station.

2.2. Sample preparation

To ensure a deformation-free surface, oxygen-loaded foils were cold embedded in epoxy, ground using sequentially finer sandpaper down to 4000#. Hereafter, polishing with 3 and 1 μm diamond suspensions was performed, and final polished occurred in neutral and basic mixtures of 0.3 μm silica particles, for 5 and 1 min, respectively. Leftover silica particles were removed with cotton and water, with no ultra-sonic cleaning being used.

[1] In this implementation constants relating to the indenter shape in the original OP analysis are determined by fitting.
[2] The MATLAB code is included as Supplementary material.

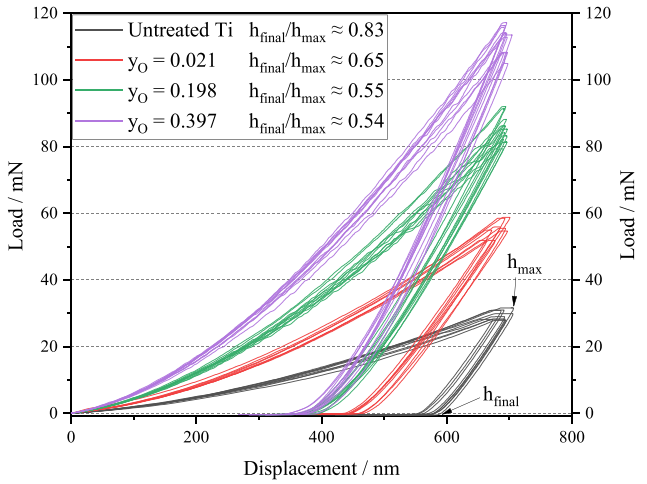

Fig. 2. Loading-unloading curves for indents made on cross-sections of untreated Ti and oxygen containing foils.

2.3. Nanoindentation

Nanoindentations were performed on cross-sections of the foils using a diamond Berkovich indenter on a NHT^2 nano-indenter from CSM Instruments. Calibration measurements of the apparatus were performed on fused silica to determine the coefficients in the polynomial of the area function (see Eqs. 1–4). A constant indentation depth of about 700 nm was aimed for to minimize indentation size effect. The applied loads ranged from 30 to 115 mN, depending on sample hardness. The holding time at the maximum load was 5 s. Both the loading and unloading of the Berkovich indenter was attained within about 21 s. The loading/unloading parts of the load-displacement curves were inspected for discontinuities/anomalies, which would indicate indents in the vicinity of a grain boundary or crack formation [1]. Such indentations were excluded from the data presented. After this exclusion 8–11 accepted indents remain for each sample. The contact point for each accepted indent was corrected by visual inspection of the curves. The slope of the unloading curves was determined by fitting a straight line to the unloading curve in the interval 98–40% of the maximum load.

2.4. Atomic force microscopy

Atomic force micrographs (AFM) were recorded on an Agilent (later Keysight) SPM 5500 equipped with an N9521A scanner (approximately 80 μm × 80 μm) and a MAC Mode AC controller. Measurements were performed in contact mode (probe: DNP-S10, Bruker). Images were recorded using PicoScan software and analyzed using the image analysis software Gwyddion. Area fitting of indents made by the Berkovich indenter was performed using 'Analyze Imprint' in Gwyddion. The software fits the AFM data to the shape of a Berkovich indenter [23] with a reference plane tolerance of 1.0% and an angle tolerance of the half-apex angle of 8°. Three scans were performed on each indent both in forward and reverse mode; the scans exhibiting least anomalies were used.

3. Results

3.1. Loading-unloading curves

The loading-unloading curves for the indents are shown in Fig. 2. The force displacement behavior is highly influenced by the increasing oxygen content, where the load needed to attain a displacement of approx. 700 nm changes systematically from about 30 mN to 115 mN with increasing oxygen content. The slope of the unloading curve, which

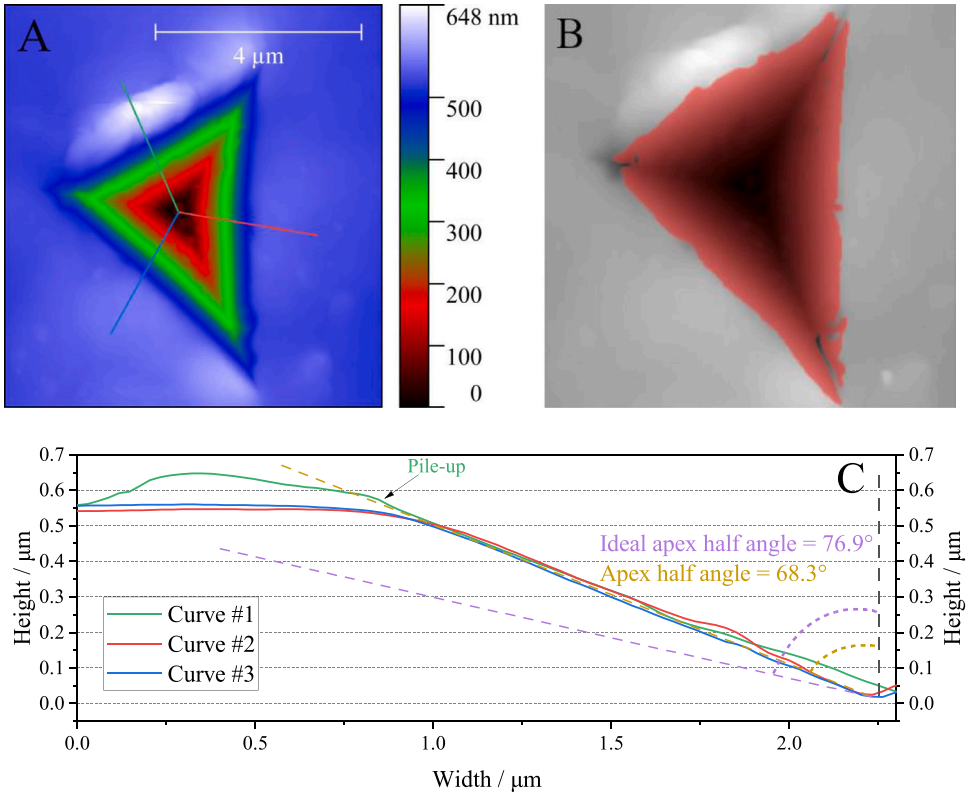

Fig. 3. (A) AFM image of indent #5 for the untreated Ti, with anisotropic pile-up. (B) Show the visual representation of the indent fit from Gwyddion. (C) The cross-sectional curves of the drawn lines in (A), with different axis units for better visualization with inserted apex half angle from equal axis figure (orange) and a reference half angle (purple).(For interpretation of the references to color in this figure legend, the reader is referred to the web version of this article.)

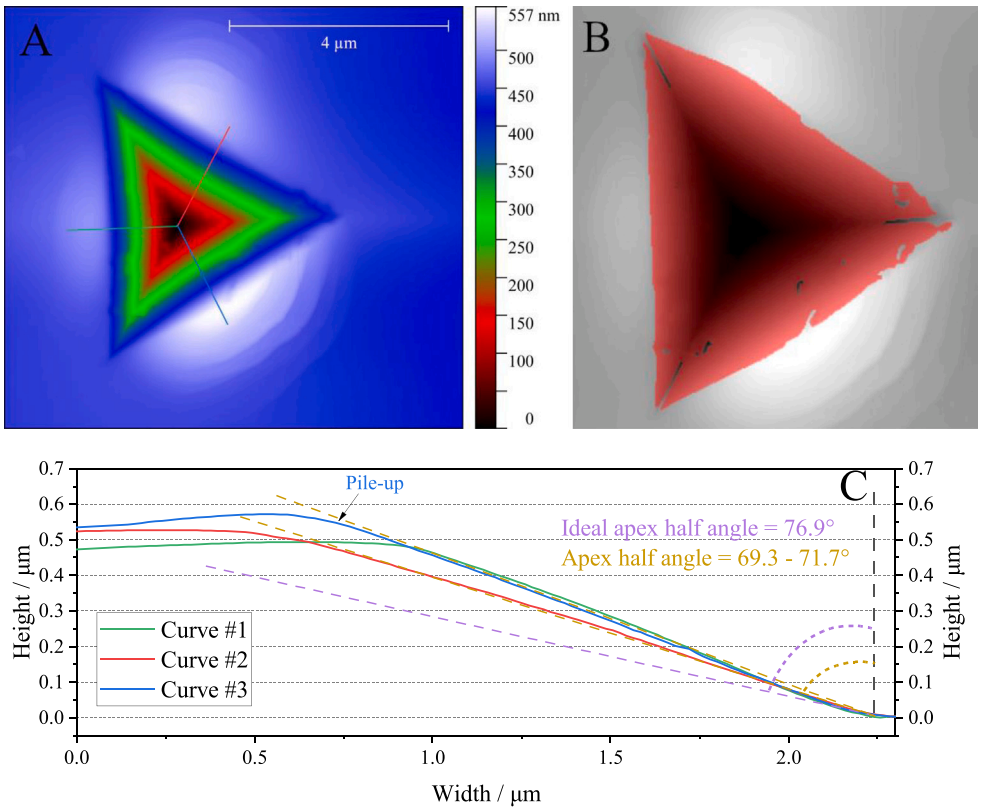

Fig. 4. (A) AFM image of indent #5 for $y_O = 0.021$. (B) Show the visual representation of the indent fit from Gwyddion. (C) The cross-sectional curves of the drawn lines in (A), with different axis units for better visualization with inserted apex half angle from equal axis figure (orange) and a reference half angle (purple).(For interpretation of the references to color in this figure legend, the reader is referred to the web version of this article.)

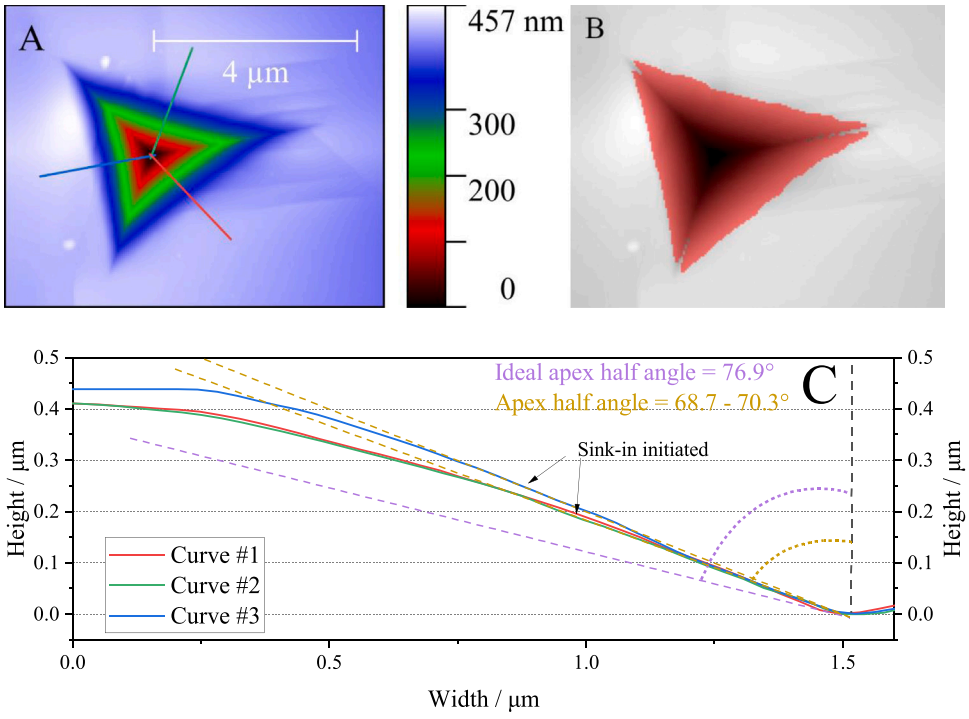

Fig. 5. (A) AFM image of indent #11 for $y_O = 0.397$, with sink-in being detected. (B) Show the visual representation of the indent fit from Gwyddion. (C) The cross-sectional curves of the drawn lines in (A), with different axis units for better visualization with inserted apex half angle from equal axis figure (orange) and a reference half angle (purple).(For interpretation of the references to color in this figure legend, the reader is referred to the web version of this article.)

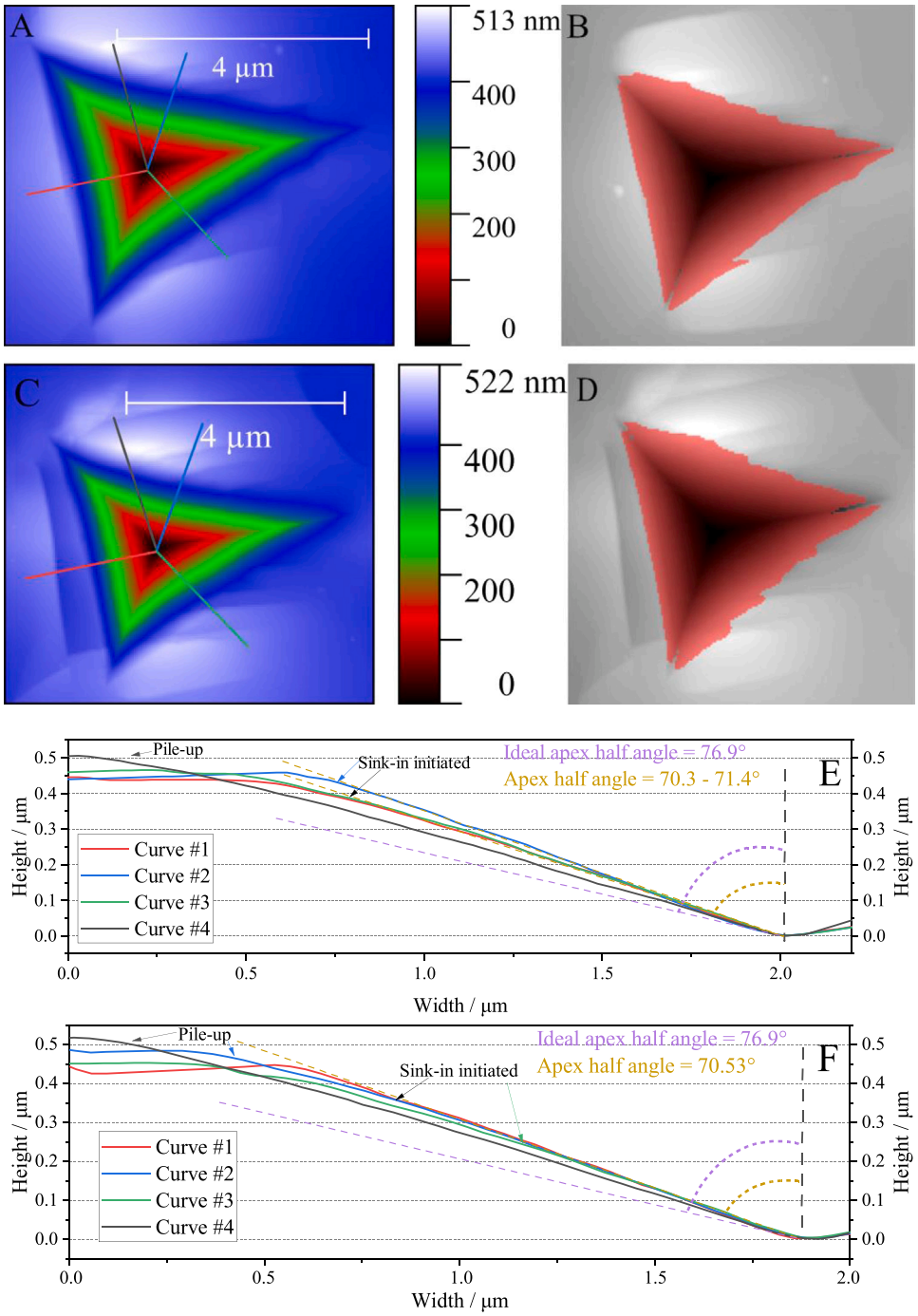

Fig. 6. AFM images of indent #6 (A) and indent #8 (C) for $y_O = 0.397$. (B) and (D) displays the Gwyddion fits for (A) and (C), respectively. Corresponding cross-sectional curves of the drawn lines in (E) for (A) and (F) for (B), with different axis units for better visualization with inserted apex half angle from equal axis figure (orange) and a reference half angle (purple).(For interpretation of the references to color in this figure legend, the reader is referred to the web version of this article.)

reflects the elastic response, also changes significantly. Increasing oxygen content leads to a much stiffer material in agreement with the literature [24]. The h_f/h_m ratios suggest that untreated Ti could display pile-up, while $y_O = 0.198$ and $y_O = 0.397$ could display sink-in. The investigated samples are representative of the behavior of various other metals and alloys. For example, untreated Ti and $y_O = 0.021$ behaves similar to Al and $y_O > 0.198$ represents hard and stiff materials, such as tetragonal martensite in steel.

3.2. Atomic force microscopy

The AFM results of a representative indent (#5 in Fig. 7) for the untreated Ti sample are presented in Fig. 3, with (A) showing the topography and the position of the line scans and (C) presenting the profile measured in the line scans. Due to the crystalline nature of metals, pileup or sink-in is typically anisotropic. In particular the h.c.p. lattice exhibits more anisotropy than the cubic lattices. In the present case, anisotropic pile-up on only one side of the indent is detected with little or no sink-in on the other sides. The apex half angle for all sides were measured to 68.3°, which should be compared to 76.9°, i.e. the apex half angle of a sharp Berkovich indenter [25]. The difference indicates a significant elastic response. The constant angle shows that contact between indenter and indented material is maintained during unloading. The area fit from Gwyddion for indent #5 is shown in (B) and illustrates that also the anisotropic pile-up is included.

The AFM scan, indent fit and curves are similarly presented in Fig. 4 (A-C) of indent #5 (in Fig. 7) for $y_O = 0.021$. The indent exhibits a significant amount of pile-up on one side (curve #3), and a much smaller

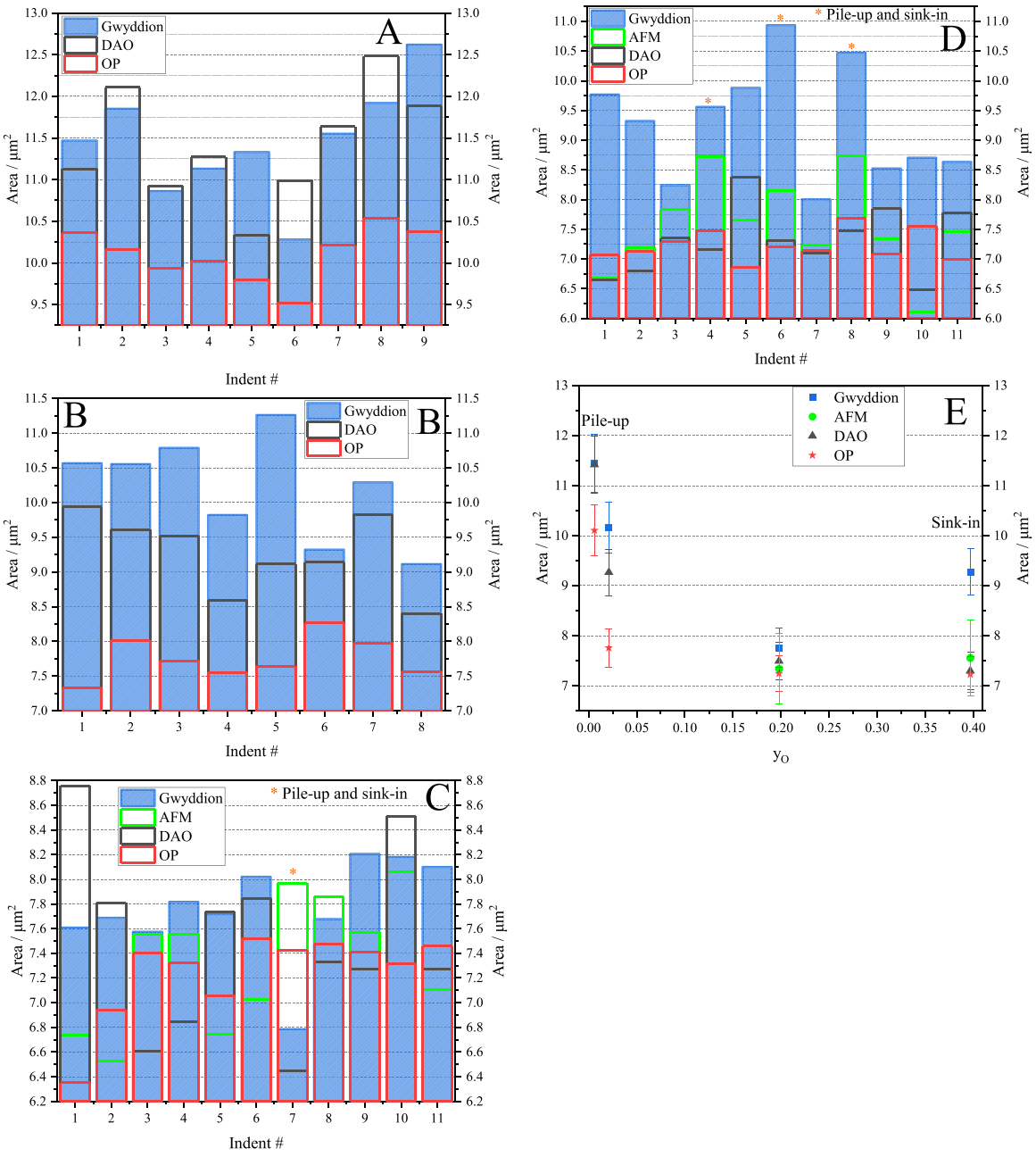

Fig. 7. The indent area determined by Dao method [18], Oliver&Pharr [1] and indent fitting from atomic force microscopy for untreated Ti (A), $y_O = 0.021$ (B), $y_O = 0.198$ (C) and $y_O = 0.397$ (D). (E) show the average area. The standard deviation is about 5% for all indents.

pile-up on another side (curve #2). The indent fit in (B) includes both these pile-ups and also captures that the pile up in one case extends along the entire indent (side 3) which is not the case for the other case (side 2). No sink-in is detected for any of indents in the $y_O = 0.021$, which all display varying degrees of pile-up. For $y_O = 0.198$ sink-in was observed for all indents, with indent #7 also exhibiting some one-sided pile-up.

The AFM scan, indent fit and curves are similarly presented in Fig. 5 (A-C) of indent #11 (in Fig. 7) for $y_O = 0.397$. The deviation of the slopes in C from linearity clearly reveals sink-in on all three sides, as also illustrated in the schematic of sink-in in Fig. 1. The point of deviation from linearity can be used to represent the extent of sink-in, and calculate the correct h_c, with $h_c = h_{max} - h_{sink\text{-}in}$, and the area with Eqs. (1–4). The average sink-in for indent #11 is about 235 nm as an example, yielding a h_c of about 465 nm. Because the area is not linear in h_c the average area is calculated as the mean of three areas calculated with the h_c values for each of the three sides, yielding 7.1 µm^2. The Gwyddion fit in (B) on the other hand includes the sink-in regions and thus overestimates the area.

AFM scans and curves for indents #6 and #8 (in Fig. 7) in the same material are shown in Fig. 6. Both indents display a complex combination of sink-in and pile-up. The blue and gray curves (curves 2 and 4) reveal both sink-in and pile-up on the same side. The combination of both behaviors complicates the determination of the indent areas. The Gwyddion fit function results in very large areas for these indents, as illustrated in the fits in Fig. 6 (B) and (D) for #6 and #8, respectively.

3.3. Comparison of indent areas

The indent areas determined by Gwyddion fitting and the OP and Dao methods for all four materials are shown in Fig. 7. While the areas of the individual indents in the same sample exhibit some variation for all

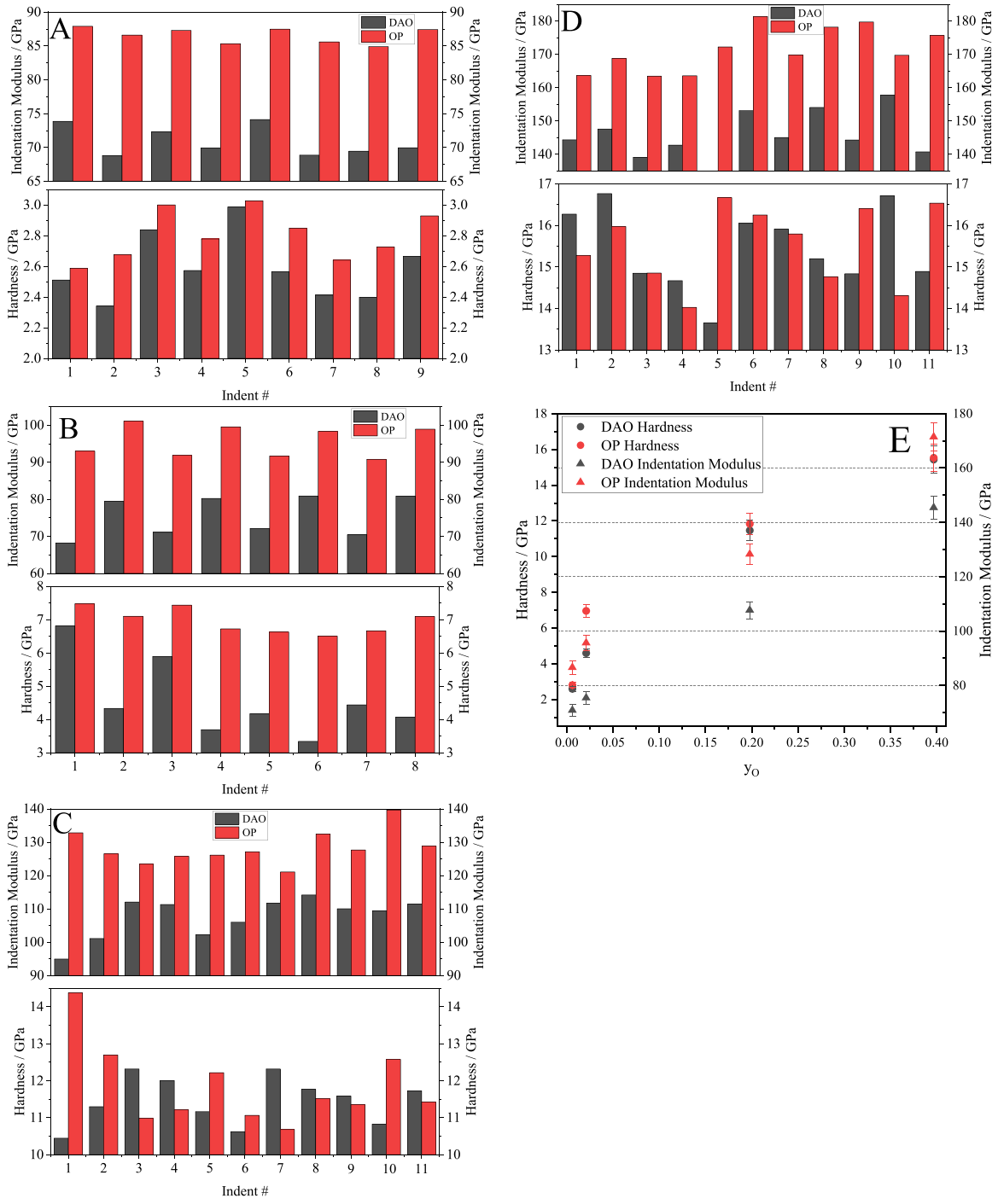

Fig. 8. The hardness and indentation modulus from Dao method [18] and Oliver&Pharr [1] for untreated Ti (A), $y_O = 0.021$ (B), $y_O = 0.198$ (C) and $y_O = 0.397$ (D). (E) Averaged values for hardness and indentation modulus. The standard deviation for hardness and indentation modulus for both methods is about 5% and 3%, respectively.

three methods, the mean values in (E) display a clear trend. Although the indents in all four materials have approximately the same penetration depth during loading, it is clear that the areas determined by Dao and OP decrease with increasing oxygen content whereas the areas from the Gwyddion fit exhibit a minimum at intermediate oxygen content. At this intermediate content all three methods give the same area within the error bars, which also matches the area from AFM corrected for sink-in as described in Section 3.2. At no or low oxygen content the areas from the OP method lie significantly lower than the other two, whereas the area from the Gwyddion method is substantially higher than the three others at the highest oxygen content. These observations also hold in general at the level of individual indents.

4. Discussion

4.1. Pile-up and sink-in effects

The decreasing areas from Dao and OP with increasing oxygen content in spite of similar penetration depth (h_m) are caused by the different properties of the materials, which is also evident from the AFM observations. For low oxygen content pile-up is dominant, whereas complex sink-in effects are observed for the highest concentrations. The

Dao method has been specifically developed for materials exhibiting pile-up and the fact that the areas from this method and the Gwyddion fit agree shows that the method is quite successful. Pile-up is not accounted for in the OP method, meaning that it consistently underestimates the area. On the other hand, the OP method is developed based on sink-in effects and thus reassures that the Dao and OP methods arrive at similar areas as the sink-in corrected AFM analysis for the samples where sink-in is observed. The commonly employed threshold of 0.7 for the ratio of the final depth (h_f) to the total depth (h_m) to distinguish between pile-up and sink-in proved a reasonable rule of thumbs.

4.2. Hardness and indentation modulus

The hardness and elastic modulus for the four samples are displayed in Fig. 8, determined using the OP and Dao methods. Due to uncertainties in the determination of the Poisson ratio of the oxygen containing titanium alloys, the term indentation modulus is employed instead of Young's modulus. In the calculations a Poisson ratio of 0.3 was assumed. On average hardness values obtained by the two methods are similar within the error bars except for sample B, which was one of the samples exhibiting pile-up. The difference in hardness is larger than what can be explained by the determined areas in Fig. 7. Noting that the areas determined for sample A also differ substantially while the hardnesses do not, and that the indentation moduli from the OP method are consistently higher, it must be concluded that although area determination is critical, also other factors inherently associated with the two methods affect the mechanical data.

4.3. Anisotropy

The variations between indentations in the same material is ascribed to the crystalline nature, which yields mechanical anisotropy. Apart from the fact that the hardness and indentation moduli depend on crystallographic orientation, the crystalline character also has implications for the pile-up/sink-in behavior. This is likely to be the origin of the complex mixture of pile-up and sink-in observed in many indents, in particular at high oxygen content. Even truly axisymmetrical indenters cause such anisotropy. For the Berkovich indenter the behavior depends critically on how the indentation direction is oriented with respect to the lattice of the grain probed [20]. The effect of crystallinity on the relative suitability of the Dao and OP methods is beyond the scope of this study. Nevertheless, it is observed that the error bars on the average quantities for the two methods are of comparable magnitude.

5. Conclusion

Based on the comparisons between the areas determined by the methods of Oliver&Pharr and Dao and AFM measurements the following conclusions are drawn:

- The AFM measurements are a good diagnostic tool to identify the pile-up and sink-in phenomena, which can be quite complex due to anisotropy of the material. Fitting of the area using the Gwyddion algorithm is possible in case of pile-up, whereas the area is overestimated for sink-in. For sink-in, a simple correction method appears to give a more precise value for the indentation area.
- The Dao method gives areas in agreement with those obtained by the Gwyddion fit in case of pile up. This is consistent with the reference materials used for developing the Dao method, i.e. metals typically exhibiting pile up.
- The Dao and the OP methods give similar areas in case of sink-in, which also agree with the areas from AFM after correction for sink-in. This was also the case for samples exhibiting a complex mixture of pile up and sink in.
- A fairly large number of indents is needed to average out the complexity of specific indents caused by crystallinity.

CRediT authorship contribution statement

Frederik Bojsen Kværndrup: Conceptualization, Methodology, Formal analysis, Validation, Investigation, Visualization, Project administration, Writing – original draft, Writing – review & editing. **Christian Engelbrekt:** Investigation, Methodology, Formal analysis, Resources. **Ömer C. Kücükyildiz:** Investigation, Methodology, Software, Formal analysis, Validation. **Marcel A.J. Somers:** Writing – review & editing. **Thomas L. Christiansen:** Funding acquisition, Project administration, Resources, Conceptualization, Methodology, Supervision, Writing – original draft, Writing – review & editing. **Grethe Winther:** Resources, Conceptualization, Methodology, Supervision, Writing – original draft, Writing – review & editing.

Declarations

Funding The work has been carried out with financial support from the Danish Council for Independent Research under grant DFF-7017-00182.

Code availability

MATLAB code is in the supplemental information.

Declaration of Competing Interest

The authors declare that they have no known competing financial interests or personal relationships that could have appeared to influence the work reported in this paper.

Data Availability

The datasets generated during and/or analysed during the current study are not publicly available due to time constraints but are available from the corresponding author on reasonable request.

Appendix A. .Supporting information

Supplementary data associated with this article can be found in the online version at doi:10.1016/j.mtcomm.2022.103218.

References

[1] W.C. Oliver, G.M. Pharr, An improved technique for determining hardness and elastic modulus using load and displacement sensing indentation experiments, J. Mater. Res. 7 (1992) 1564–1583, https://doi.org/10.1557/JMR.1992.1564.
[2] W.C. Oliver, G.M. Pharr, Measurement of hardness and elastic modulus by instrumented indentation: advances in understanding and refinements to methodology, J. Mater. Res. 19 (2004) 3–20, https://doi.org/10.1557/jmr.2004.19.1.3.
[3] A.C. Fischer-Cripps, Mechanical Engineering Series: Nanoindentation, 2011. https://doi.org/10.1007/978–1-4419–9872-9.
[4] H. Li, A. Ghosh, Y.H. Han, R.C. Bradt, The frictional component of the indentation size effect in low load microhardness testing, J. Mater. Res. 8 (1993) 1028–1032, https://doi.org/10.1557/JMR.1993.1028.
[5] A. Bolshakov, G.M. Pharr, Influences of pileup on the measurement of mechanical properties by load and depth sensing indentation techniques, J. Mater. Res. 13 (1998) 1049–1058, https://doi.org/10.1557/JMR.1998.0146.
[6] L. Charleux, V. Keryvin, M. Nivard, J.P. Guin, J.C. Sanglebœuf, Y. Yokoyama, A method for measuring the contact area in instrumented indentation testing by tip scanning probe microscopy imaging, Acta Mater. 70 (2014) 249–258, https://doi.org/10.1016/j.actamat.2014.02.036.
[7] J.D. Gale, A. Achuthan, The effect of work-hardening and pile-up on nanoindentation measurements, J. Mater. Sci. 49 (2014) 5066–5075, https://doi.org/10.1007/s10853-014-8213-4.
[8] Z. Li, Y.T. Cheng, H.T. Yang, S. Chandrasekar, On two indentation hardness definitions, Surf. Coat. Technol. 154 (2002) 124–130, https://doi.org/10.1016/S0257-8972(02)00021-X.
[9] M. Mata, J. Alcalá, Mechanical property evaluation through sharp indentations in elastoplastic and fully plastic contact regimes, J. Mater. Res. 18 (2003) 1705–1709, https://doi.org/10.1557/JMR.2003.0234.

[10] N. Moharrami, S.J. Bull, A comparison of nanoindentation pile-up in bulk materials and thin films, Thin Solid Films 572 (2014) 189–199, https://doi.org/10.1016/j.tsf.2014.06.060.
[11] N.X. Randall, C. Julia-Schmutz, Evolution of contact area and pile-up during the nanoindentation of soft coatings on hard substrates, Mater. Res. Soc. Symp. Proc. 522 (1998) 21–26, https://doi.org/10.1557/PROC-522-21.
[12] L.I. Krenev, S.S. Volkov, E.V. Sadyrin, T.I. Zubar', S.A. Chizhik, Mechanical material tests by the nanoindentation method at various indenter and specimen temperatures, J. Eng. Phys. Thermophys. 91 (2018) 594–600, https://doi.org/10.1007/s10891-018-1780-5.
[13] I.I. Argatov, Depth-sensing indentation of a transversely isotropic elastic layer: second-order asymptotic models for canonical indenters, Int. J. Solids Struct. 48 (2011) 3444–3452, https://doi.org/10.1016/j.ijsolstr.2011.08.011.
[14] A.S. Vasiliev, S.S. Volkov, E.V. Sadyrin, S.M. Aizikovich, Simplified analytical solution of the contact problem on indentation of a coated half-space by a conical punch, Mathematics 8 (2020), https://doi.org/10.3390/MATH8060983.
[15] T. Chudoba, N. Schwarzer, F. Richter, Determination of elastic properties of thin films by indentation measurements with a spherical indenter, Surf. Coat. Technol. 127 (2000) 9–17, https://doi.org/10.1016/S0257-8972(00)00552-1.
[16] Y.H. Lee, J.H. Hahn, S.H. Nahm, J.I. Jang, D. Kwon, Investigations on indentation size effects using a pile-up corrected hardness, J. Phys. D. Appl. Phys. 41 (2008), https://doi.org/10.1088/0022-3727/41/7/074027.
[17] M.F. Doerner, W.D. Nix, A method for interpreting the data from depth-sensing indentation instruments, J. Mater. Res. 1 (1986) 601–609, https://doi.org/10.1557/JMR.1986.0601.
[18] M. Dao, N. Chollacoop, K.J. Van Vliet, T.A. Venkatesh, S. Suresh, Computational modeling of the forward and reverse problems in instrumented sharp indentation, Acta Mater. 49 (2001) 3899–3918, https://doi.org/10.1016/S1359-6454(01)00295-6.
[19] H.R. Ogden, R.I. Jaffee, The effects of carbon, oxygen, and nitrogen on the mechanical properties of titanium and titanium alloys, 1955. https://doi.org/10.2172/4370612.
[20] C. Zambaldi, D. Raabe, Plastic anisotropy of γ-TiAl revealed by axisymmetric indentation, Acta Mater. 58 (2010) 3516–3530, https://doi.org/10.1016/j.actamat.2010.02.025.
[21] J.L. Murray, H.A. Wriedt, Murray, Wriedt - 1987 - The O-Ti (oxygen-titanium) system, Bull. Alloy Ph. Diagr. 8 (1987) 148–165.
[22] F.B. Kværndrup, Ö.C. Kücükyildiz, G. Winther, M.A.J. Somers, T.L. Christiansen, Extreme hardening of titanium with colossal interstitial contents of nitrogen and oxygen, Mater. Sci. Eng. A 813 (2021), 141033.
[23] Gwyddion source code, (n.d.). ⟨http://gwyddion.net/download.php⟩ (Accessed 25 March 2021).
[24] H. Conrad, Effect of interstitial solutes on the strength and ductility of titanium, Prog. Mater. Sci. 26 (1981) 123–403, https://doi.org/10.1016/0079-6425(81)90001-3.
[25] A. Karimzadeh, S.S. Rahimian Koloor, M.R. Ayatollahi, A.R. Bushroa, M. Yahya, Assessment of nano-indentation method in mechanical characterization of heterogeneous nanocomposite materials using experimental and computational approaches, Sci. Rep. 9 (2019) 15763, https://doi.org/10.1038/s41598-019-51904-4.